Heat transport analysis in high density NBI plasmas of Heliotron J

X. X. Lu[1], S. Kobayashi[2], R. Seki[3], K. Y. Watanabe[3], D. L. Yu[4], K. Nagasaki[2], S. Kado[2], H. Okada[2], T. Minami[2], S. Ohshima[2], S. Yamamoto[2], A. Ishizawa[1], Y. Nakamura[1], S. Konoshima[2], T. Mizuuchi[2]

[1]*Graduate School of Energy Science, Kyoto University, Uji, 611-0011, Japan*
[2]*Institute of Advanced Energy, Kyoto University, Gokasho, Uji, 611-0011, Japan*
[3]*National Institute for Fusion Science, Toki, Gifu, 509-5292, Japan*
[4]*Southwestern Institute of Physics, Chengdu 610041, China*

E-mail: lu.xiangxun.84m@st.kyoto-u.ac.jp

1. Introduction

A high density NBI plasma experiment with High Intensity Gas Puffing (HIGP) technique has been demonstrated in Heliotron J [1, 2]. Using the fuelling scenarios, a higher plasma stored energy (W_p) has been achieved with a higher plasma density, however, electron/ion temperature profile were not modified drastically on different density discharges. To study the characteristics of the heat transport in such high density plasmas, we apply a heat transport analysis using a one-dimensional diffusive transport module, so called TR-snap code [3], based on the power balance analysis, and compare the heat transport coefficient χ for electrons and ions on different density discharges. The NBI power absorption and the heat transport are analysed, and the dependence on density are discussed in this article.

2. Experimental setup

Heliotron J is a medium sized (R=1.2m, a=0.2m) helical-axis heliotron device. In the experiment reported here, the plasmas were started up by 70GHz ECRH and sustained by balanced-NBI heating with total port-through power of 1MW. A high density plasma is generated by the HIGP method, in which gas puffing is applied with short-pulse (15ms) and high fuelling rate several times higher than that of the conventional one. To study the dependence of the heat transport on the electron density, we compared three electron density cases (high, medium and low densities) under the quasi-steady state phase (maximum W_p) as shown in Table 1.

Shot number	$\bar{n}_e$ ($\times 10^{19}/m^3$)	Note
#60514	3.5	High density
#60975	1.3	Medium density
#60513	0.9	Low density

Table 1. The discharge information in this paper

In this experiment, the line-averaged electron density ($\bar{n}_e$), was measured with a far infrared-laser interferometer system, and the electron density (n_e), electron temperature profiles (T_e) and ion temperature profiles (T_i), were measured with a Nd: YAG Laser Thomson scattering and a charge-exchange recombination spectroscopy systems, respectively.

3. Experiment results and heat transport analysis

The profiles of the electron density, electron and ion temperatures are shown in Fig. 1. The profile shapes for both T_e and T_i are similar with different plasma densities. And the electron temperature profile is more peaked than ion's, which implies large electron temperature gradient at core and large ion temperature gradient at peripheral region. Under the density range, the electron temperature is not sensitive to the density, and the ion temperature slightly decreases with electron density. The NBI power absorption is evaluated by FIT-3D code [4], which consist of the fast ion calculation by NBI using Monte-Carlo method. The profile of NBI power density absorbed in electrons (P_e^{NBI}) and ions (P_i^{NBI}) are shown in Fig. 2(a) and (b). Both P_e^{NBI} and P_i^{NBI} increase with electron density, due to the reduction of the NBI shine-through loss. As shown in Fig. 2(c), the total absorbed NBI power ($\int P^{NBI} dV$) for both electrons and ions in the high density plasma is twice as high

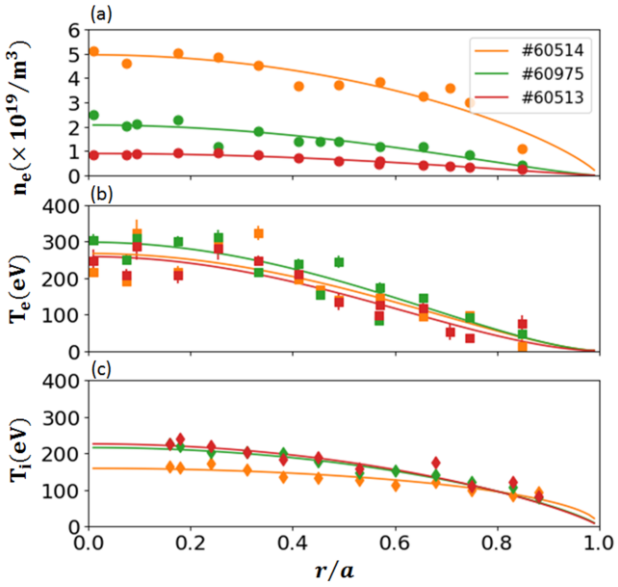

Figure 1. n_e (a), T_e (b) and T_i (c) profile of the discharges in Table 1

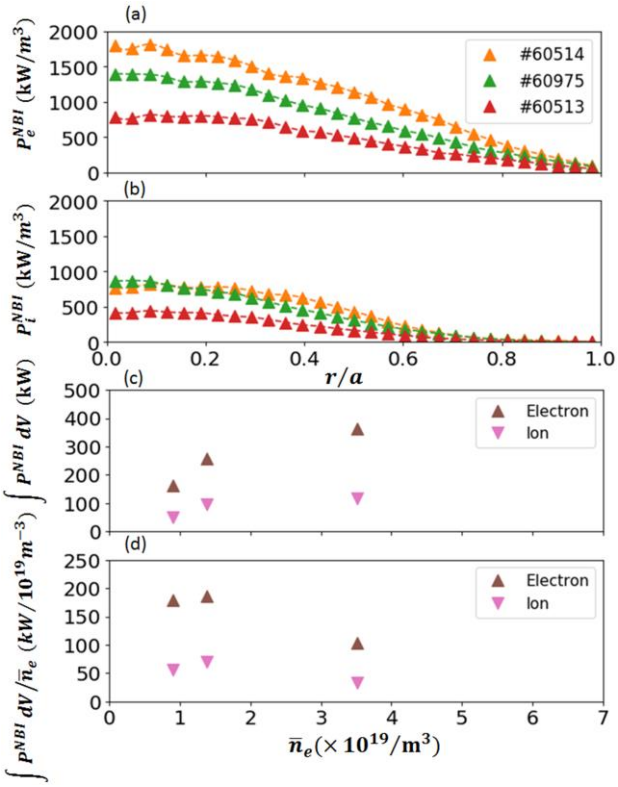

Figure 2. NBI power density absorbed by electron (a) and ion (b), density dependence of total absorbed NBI power (c) and density normalized NBI Power (d)

as that in the low density one. On the other hand, the total absorbed NBI power normalized by $\bar{n}_e$, $\int P^{NBI}dV/\bar{n}_e$ decreases significantly under the high density plasma condition as shown in Fig. 2(d). In the case of high density plasma (#60514), the ion temperature slightly decreases as compared with the low density plasma (#60513) case, while the normalized NBI heating power decreases more than 60% for both electrons and ions, which may be concerned with the improvement of the heat transport.

To clarify the heat transport characteristics of the high density NBI plasmas, the TR-snap code is applied to evaluate the effective heat transport coefficients. The effective heat transport coefficient χ_j (j: particle species) is given as the following equation,

$$\chi_j = -\frac{\int P_j^{NBI}(\rho)dV}{\langle|\nabla\rho|^2\rangle\frac{dV}{d\rho}n_j(\rho)\frac{\partial T_j(\rho)}{\partial\rho}}.$$

Here, the effect of particle flux, energy equipartition and radiation loss are ignored.

The profiles of effective electron and ion heat transport coefficients, χ_e and χ_i are shown in Fig. 3(a) and 3(b). In this calculation, the electron temperature gradient is large in the region of $0.2 \leq r/a \leq 0.6$, which concerned with a flat χ_e. On the other hand, the ion temperature gradient is small at the core region but increased significantly at the peripheral region, which concerned with a lower χ_i near the peripheral region (r/a=0.7) than that at core region (r/a=0.2).

In the high density condition (#60514), both χ_e and χ_i decreases in the region of $0.2 \leq r/a \leq 0.75$. Fig. 4(a)-(c) shows the density dependence of χ_e and χ_i at three radial positions. The electron heat transport coefficient decreases significantly with increasing electron density. In high density case, no significant variation in electron temperature, however the density normalized NBI power decreases by more than 60% compared with the low density case (#60513), hence the electron

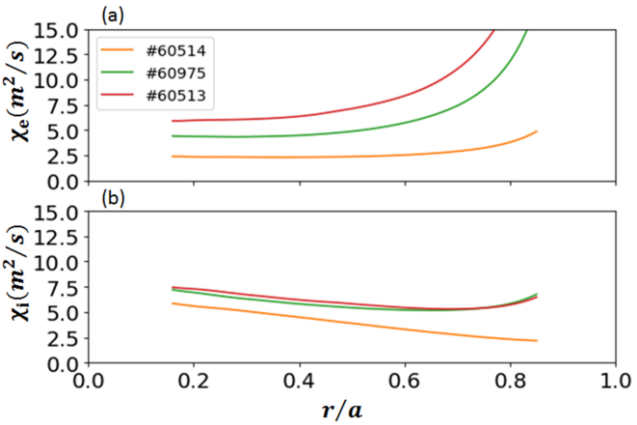

Figure 3. χ_e (a) and χ_i profile (b) of plasmas in table 1

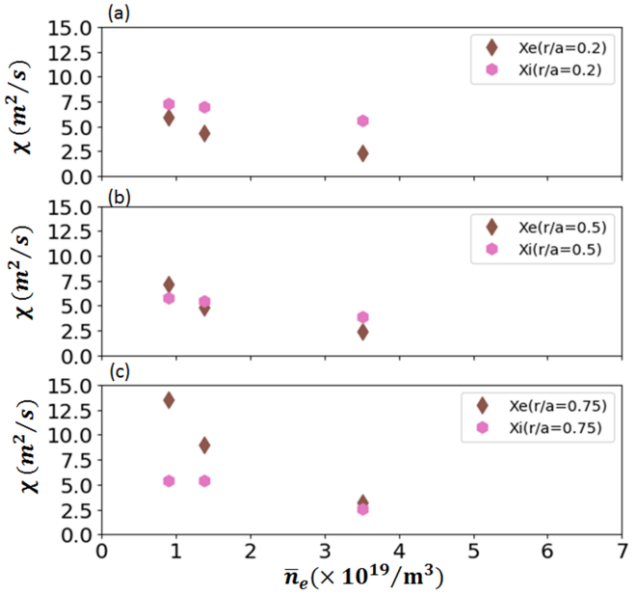

Figure 4. The density dependence of χ_e and χ_i at r/a=0.2 (a), r/a=0.5 (b) and r/a=0.75 (c)

heat transport is improved significantly and indicating strong density dependence. At the peripheral region, the electron heat transport is much improved in the case of the high density plasma. On the other hand, with a smaller ion temperature gradient, the ion heat transport coefficient decreases slightly with the electron density, and the improvement of χ_i is not so impressive in the case of high density condition, indicating weak density dependence. These results show that both electron and ion heat transports at the region of $0.2 \leq r/a \leq 0.75$ are improved with electron density, and the electron heat transport has strong density dependence.

4. Summary

The density dependence of heat transport in NBI plasmas is studied based on the NBI absorption calculation and the heat transport analysis. The NBI heating power calculation shows the NBI absorbed power normalized by the electron density decreases with electron density. The heat transport analysis shows both χ_e and χ_i in the region of $0.2 \leq r/a \leq 0.75$ decreases with the electron density, which implies that the high density plasma has a better heat transport. The electron heat transport has strong density dependence, and χ_e is improved significantly at peripheral region in the case of high density plasma. On the other hand, the ion heat transport improvement in the high density condition is not as impressive as the electron's, which has weak density dependence.

In this article, the effect of particle flux, energy equipartition and radiation loss is ignored in the heat transport calculation. The heat transport might be overestimated since all heating energy is transferred without radiation loss. The heat transport analysis will be done with taking the effects of the particle flux, energy equipartition between electron and ion and the radiation loss into account in the next work.

Acknowledgements

The authors would like to thank the Heliotron J staff for their support of the experiments. This work was supported by NIFS/NINS under the NIFS Collaborative Research Program (NIFS10KUHL030, NIFS12KUHL051).

References

[1] T. Mizuuchi, et al., IAEA-CN-221/EX/P4-29 (2014).

[2] S. Kobayashi, et al., IAEA-CN-234/EX/P8-17 (2016).

[3] R. Seki, et al., *Plasma Fusion Res*. **6**, 2402081 (2011).

[4] S. Murakami, et al., *Fusion Technology*, **27**, 259 (1995)